Electronic Supplementary Material (ESI) for Inorganic Chemistry Frontiers.

Supporting Information

Photo- and triboluminescent robust 1D polymers made of Mn(II) halides and *meta*-caborane based bis(phosphine oxide)

Alexander V. Artem'ev,* Maria P. Davydova, Alexey S. Berezin, Taisiya S. Sukhikh, Denis G. Samsonenko

Nikolaev Institute of Inorganic Chemistry, Siberian Branch of Russian Academy of Sciences, 3, Acad. Lavrentiev Ave., 630090 Novosibirsk, Russian Federation

*E-mail: chemisufarm@yandex.ru (Alexander V. Artem'ev)

Table of content

§1. Single crystal X-ray crystallography

Single crystals of **L** and **1** were grown by slow evaporation of MeCN solutions for overnight. Crystals of **2** and **3**·CH_2Cl_2 were grown by vapor diffusion of Et_2O into a CH_2Cl_2/EtOH solution for overnight. Crystals of **3** were grown by vapor diffusion of Et_2O into a MeCN/EtOH solution for overnight.

The X-ray data and the details of the refinement are summarized in Table S1. Diffraction data for **L**, **2** and **3** were collected on an automated Agilent Xcalibur diffractometer equipped with an area AtlasS2 detector (graphite monochromator, λ(MoKα) = 0.71073 Å, ω-scans). Integration, absorption correction, and determination of unit cell parameters were performed using the CrysAlisPro program package.[1] Single crystal XRD data for **1** and **3**·CH_2Cl_2 were collected with a Bruker D8 Venture diffractometer with a CMOS PHOTON III detector and IμS 3.0 source (mirror optics, λ(MoKα) = 0.71073 Å). Absorption corrections were applied with the use of the SADABS program.[2] The structures were solved by dual space algorithm (SHELXT[3]) and refined by the full-matrix least squares technique (SHELXL[4]) in the anisotropic approximation (except H atoms). Positions of H atoms were calculated geometrically and refined in the riding model.

The crystallographic data and details of the structure refinements are summarized in Table S1. CCDC 2022607–2022609, 2035961 and 2045312 contain the supplementary crystallographic data for this paper. These data can be obtained free of charge from The Cambridge Crystallographic Data Center at http://www.ccdc.cam.ac.uk/data_request/cif

Table S1. X-Ray crystallographic data for **L**, **1**–**3** and **3**·CH_2Cl_2.

	L	**1**	**2**	**3**	**3**·CH_2Cl_2
Crystal data	2022609	2035961	2022607	2022608	2045312
Chemical formula	$C_{26}H_{30}B_{10}O_2P_2$	$C_{26}H_{30}B_{10}Cl_2MnO_2P_2$	$C_{26}H_{30}B_{10}Br_2MnO_2P_2$	$C_{26}H_{30}B_{10}I_2MnO_2P_2$	$(C_{26}H_{30}B_{10}I_2MnO_2P_2)\cdot CH_2Cl_2$
M_r	544.54	670.38	759.30	853.28	938.20
Crystal system, space group	Monoclinic, *C*2/*c*	Orthorhombic, *Pbca*	Orthorhombic, *Pbca*	Monoclinic, *Cc*	Orthorhombic, *Pca*2_1
Temperature (K)	140	150	140	150	150
a, *b*, *c* (Å)	25.4257(10), 12.5973(3), 21.3295(9)	16.4791(13), 18.4495(13), 20.8342(13)	16.7498(3), 18.5197(4), 20.8719(5)	12.42162(18), 16.3805(2), 17.6357(3)	35.4680(11), 10.5749(4), 19.2878(7)
β(°)	124.412(6)	–	–	106.1647(15)	–
V (Å^3)	5636.1(5)	6334.2(8)	6474.5(2)	3446.51(9)	7234.3(4)
Z	8	8	8	4	8
μ (mm^{-1})	0.18	0.71	3.00	2.29	2.34
Crystal size (mm)	0.26 × 0.19 × 0.16	0.22 × 0.1 × 0.05	0.53 × 0.25 × 0.10	0.23 × 0.16 × 0.13	0.32 × 0.12 × 0.05
T_{min}, T_{max}	0.988, 1.000	0.661, 0.745	0.591, 1.000	0.963, 1.000	0.616, 0.746
No. of measured, independent and observed [$I > 2\sigma(I)$] reflections	12775, 6103, 5470	52131, 6476, 5133	56203, 8022, 6924	14026, 6863, 6716	66261, 14358, 13148
R_{int}	0.014	0.071	0.026	0.017	0.056
$(\sin\theta/\lambda)_{max}$ (Å^{-1})	0.673	0.625	0.684	0.684	0.625
$R[F^2 > 2\sigma(F^2)]$, $wR(F^2)$, *S*	0.033, 0.096, 1.05	0.038, 0.096, 1.04	0.030, 0.076, 1.05	0.018, 0.044, 1.03	0.040, 0.100, 1.03

No. of reflections	6103	6476	8022	6863	14358
No. of parameters	391	388	418	418	807
No. of restraints	10	–	10	12	6
$\Delta\rangle_{max}$, $\Delta\rangle_{min}$ (e Å^{-3})	0.34, –0.33	0.34, -0.48	1.40, –1.13	0.56, –0.31	1.70, -1.21
Absolute structure parameter[5]	–	–	–	–0.024(7)	–0.005(8)

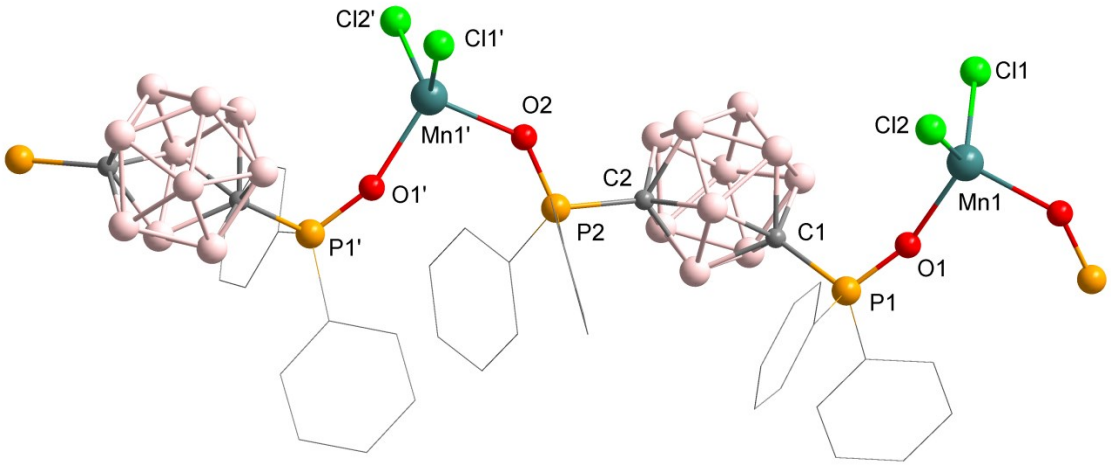

Figure S1. A fragment of the 1D chain of **1**. The H atoms are omitted. Selected bond lengths (Å) and angles (°): Mn1–Cl1 2.3135(8), Mn1–O1 2.0723(17), Mn1–Cl2 2.3227(8), Mn1–O2 2.0896(15); Cl1–Mn1–Cl2 114.04(3), O1–Mn1–O2 99.06(6), O1–Mn1–Cl1 113.34(5), O2–Mn1–Cl1 111.43(5), O1–Mn1–Cl2 112.77(5), O2–Mn1–Cl2 104.84(5). Symmetry code ('): *x*, 0.5–*y*, 0.5+*z*.

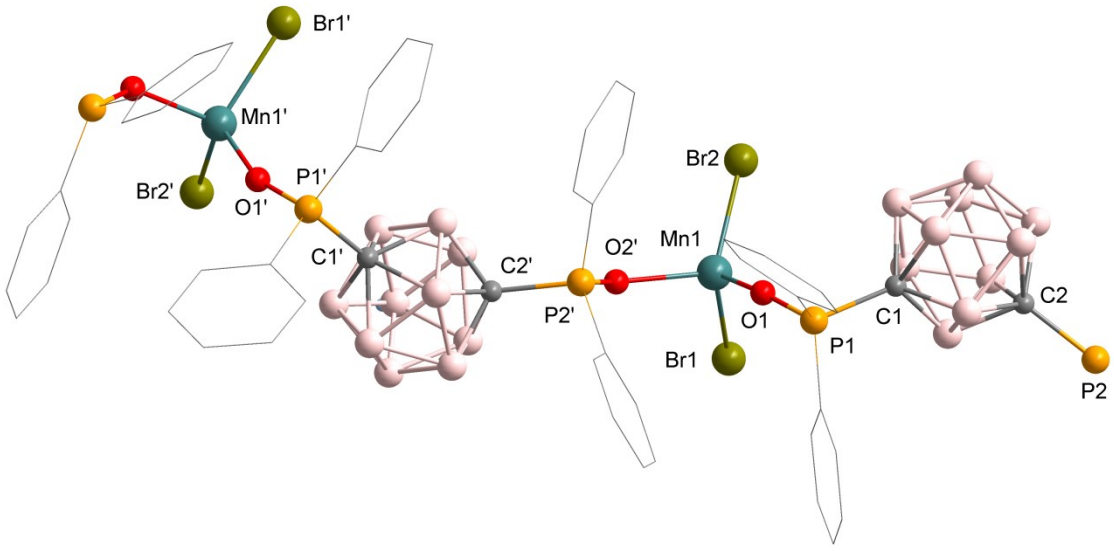

Figure S2. A fragment of the 1D chain of **2**. The H atoms are omitted. Selected bond lengths (Å) and angles (°): Mn1–Br1 2.4595(4), Mn1–Br2 2.4564(4), Mn1–O1 2.0579(13), Mn1–O2' 2.0796(13), C1–P1 1.8503(18), C2–P2 1.8428(18), P1–O1 1.4977(13), P2–O2 1.5005(13); Br2–Mn1–Br1 113.027(14), O1–Mn1–Br1 114.00(4), O1–Mn1–Br2 111.16(4), O1–Mn1–O2' 100.28(5), O2'–Mn1–Br1 104.77(4), O2'–Mn1–Br2 112.78(4). Symmetry code ('): *x*, 0.5–*y*, *z*–0.5.

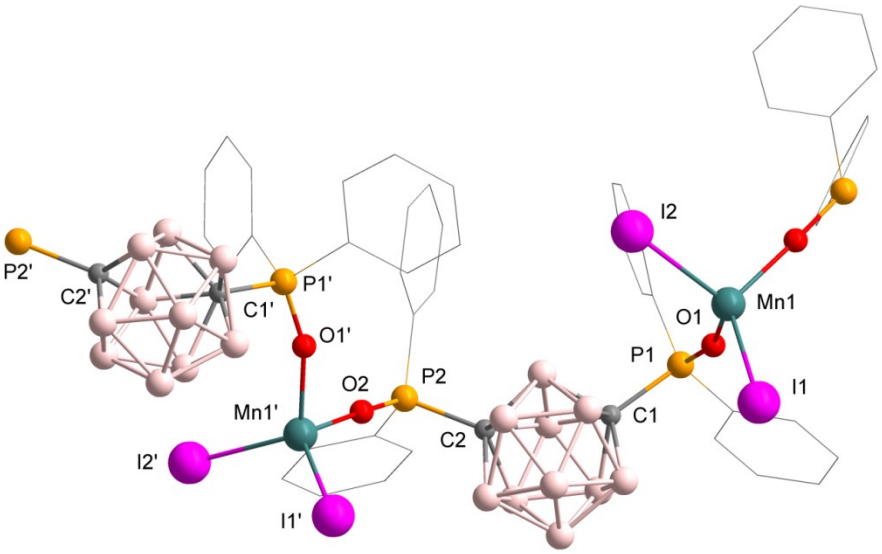

Figure S3. A fragment of the 1D chain of **3**. The H atoms are omitted. Selected bond lengths (Å) and angles (°): Mn1–I1 2.6795(5), Mn1–I2 2.6780(5), Mn1–O1 2.044(2), Mn1'–O2 2.044(2), O1–P1 1.490(2), P1–C1 1.851(3), O2–P2 1.495(2), P2–C2 1.844(3); I2–Mn1–I1 114.109(17), O1–Mn1–I1 104.33(7), O1–Mn1–I2 115.24(7), O1'–Mn1'–O2 95.27(9), O2–Mn1'–I1' 121.87(7), O2–Mn1'–I2' 104.97(6). Symmetry code ('): *x*, 1–*y*, 0.5+*z*.

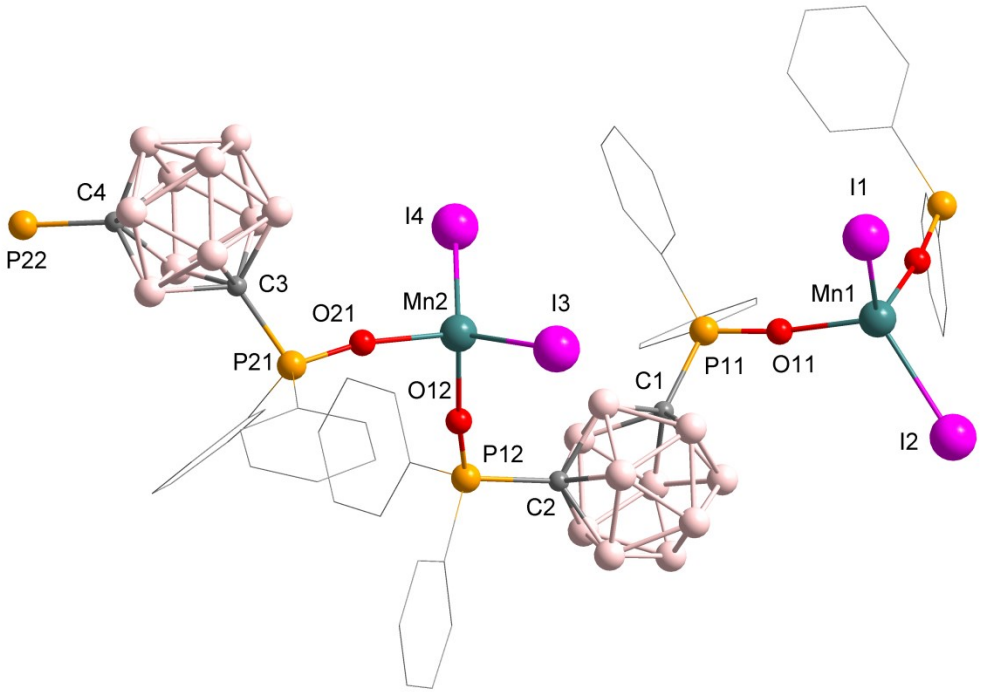

Figure S4. A fragment of the 1D chain of **3**·CH_2Cl_2. The H atoms and CH_2Cl_2 molecules are omitted. Selected bond lengths (Å) and angles (°): I1–Mn1 2.6714(14), Mn1–O11 2.030(6), I2–Mn1 2.6831(12), Mn1–O22 2.040(5), I3–Mn2 2.6783(15), Mn2–O12 2.045(6), I4–Mn2 2.6528(15), Mn2–O21 2.049(5); I1–Mn1–I2 119.45(5), I4–Mn2–I3 123.94(5), O11–Mn1–I1 107.04(17), O12–Mn2–I3 108.21(17), O11–Mn1–I2 114.33(18), O12–Mn2–I4 104.89(18), O12–Mn2–O2 100.4(3), O21–Mn2–I3 107.78(18), O21–Mn2–I4 109.08(16).

§2. Powder X-ray diffraction data

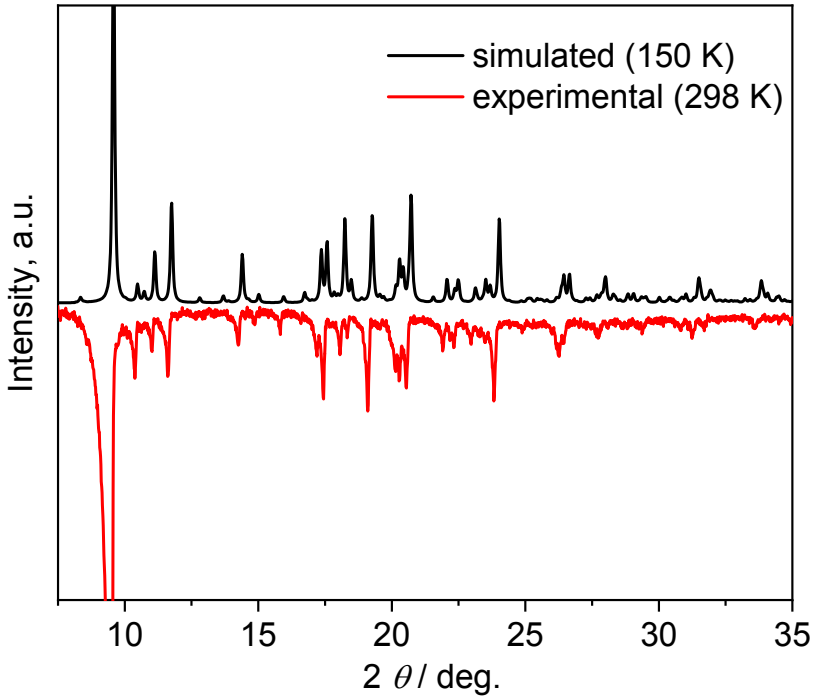

Figure S5. Experimental and simulated PXRD patterns of an as-synthesized sample of **1**.

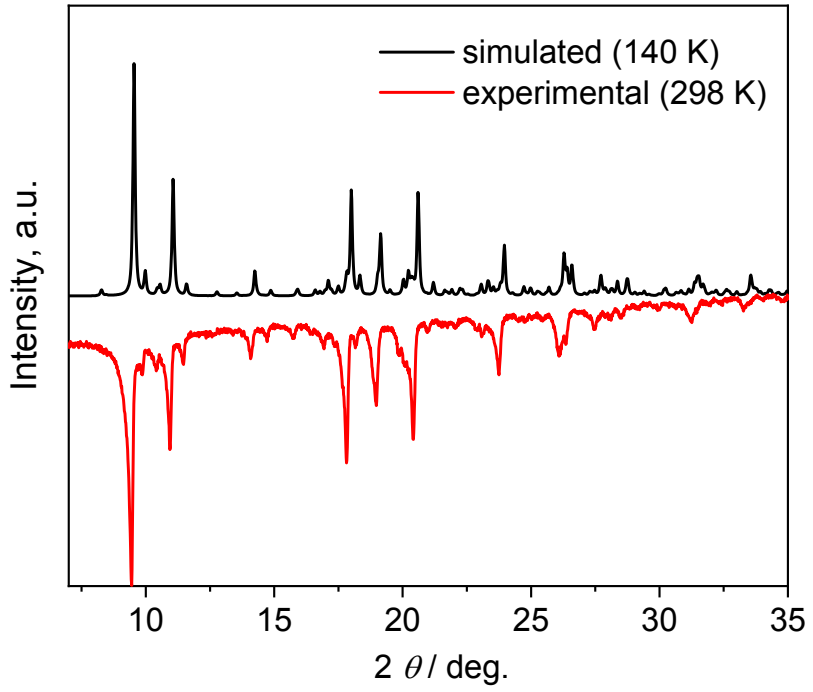

Figure S6. Experimental and simulated PXRD patterns of an as-synthesized sample of **2**.

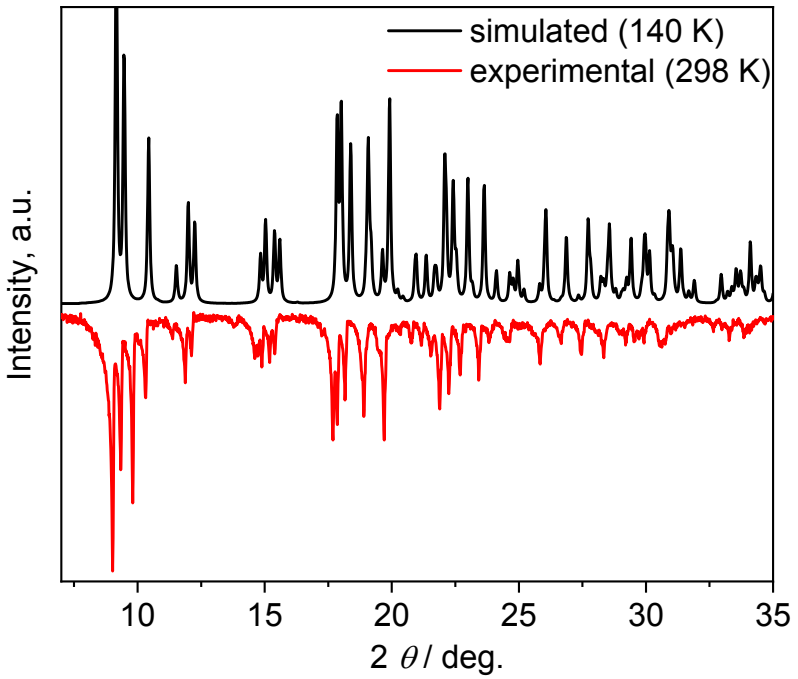

Figure S7. Experimental and simulated PXRD patterns of an as-synthesized sample of **3**.

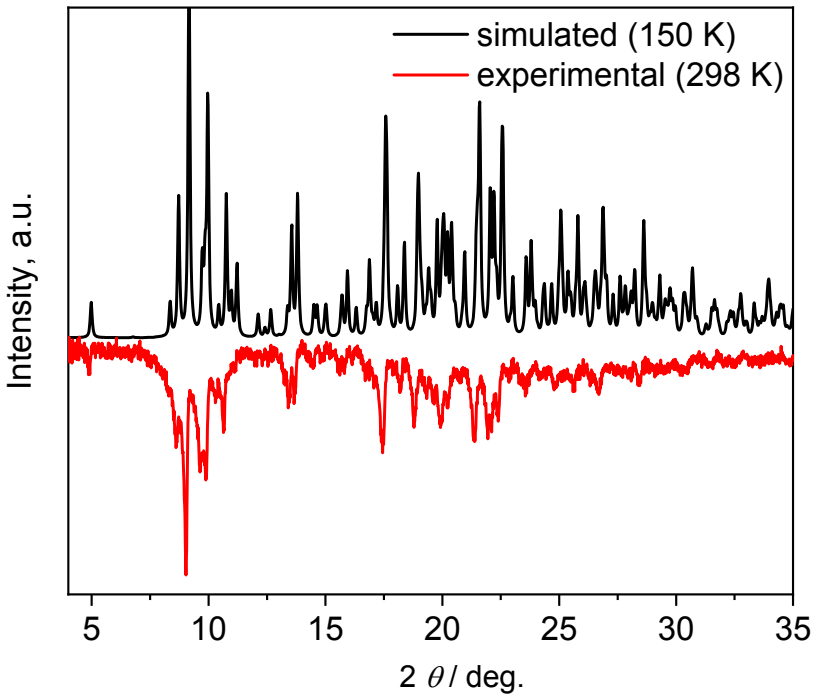

Figure S8. Experimental and simulated PXRD patterns of an as-synthesized sample of **3**·CH_2Cl_2.

§3. NMR spectra of the ligand

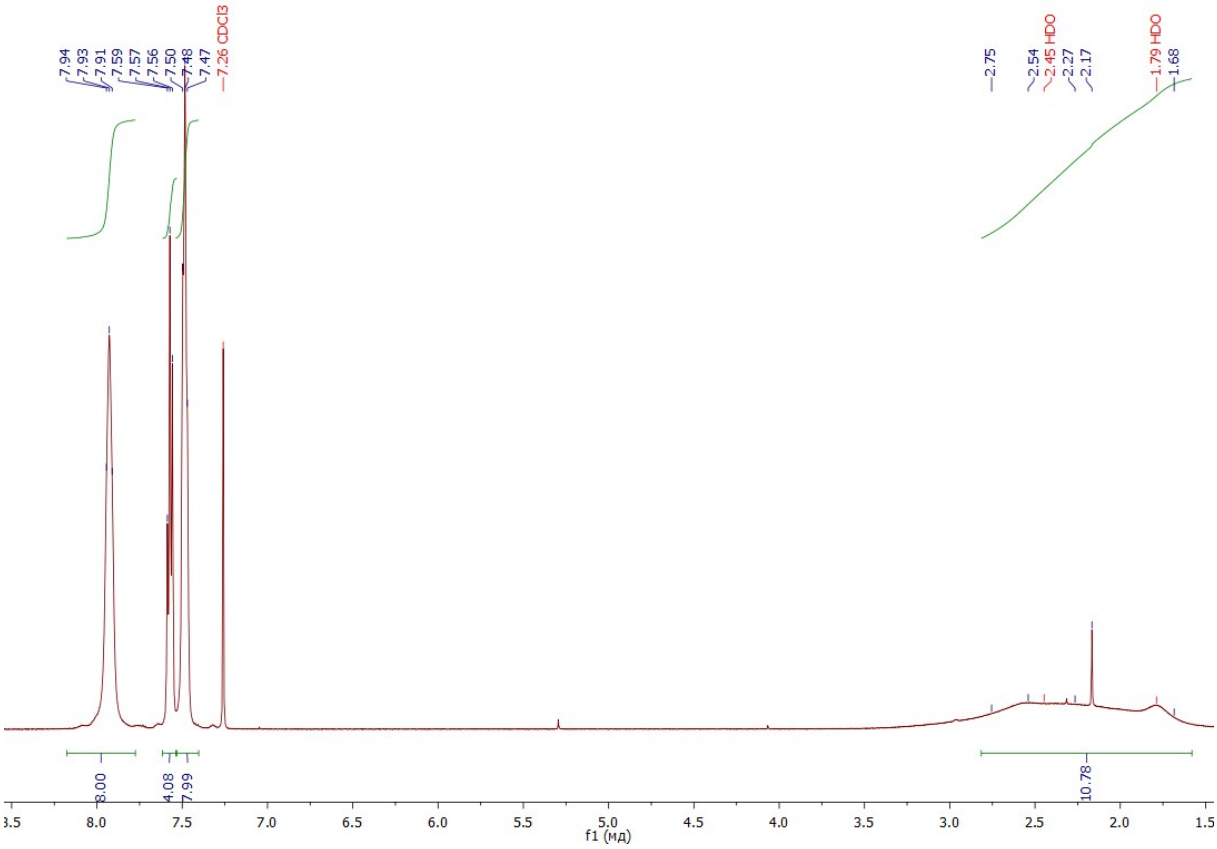

Figure S9. ^{1}H NMR spectrum of 1,7-bis(diphenylphosphinyl)-*m*-carborane (L) ($CDCl_3$).

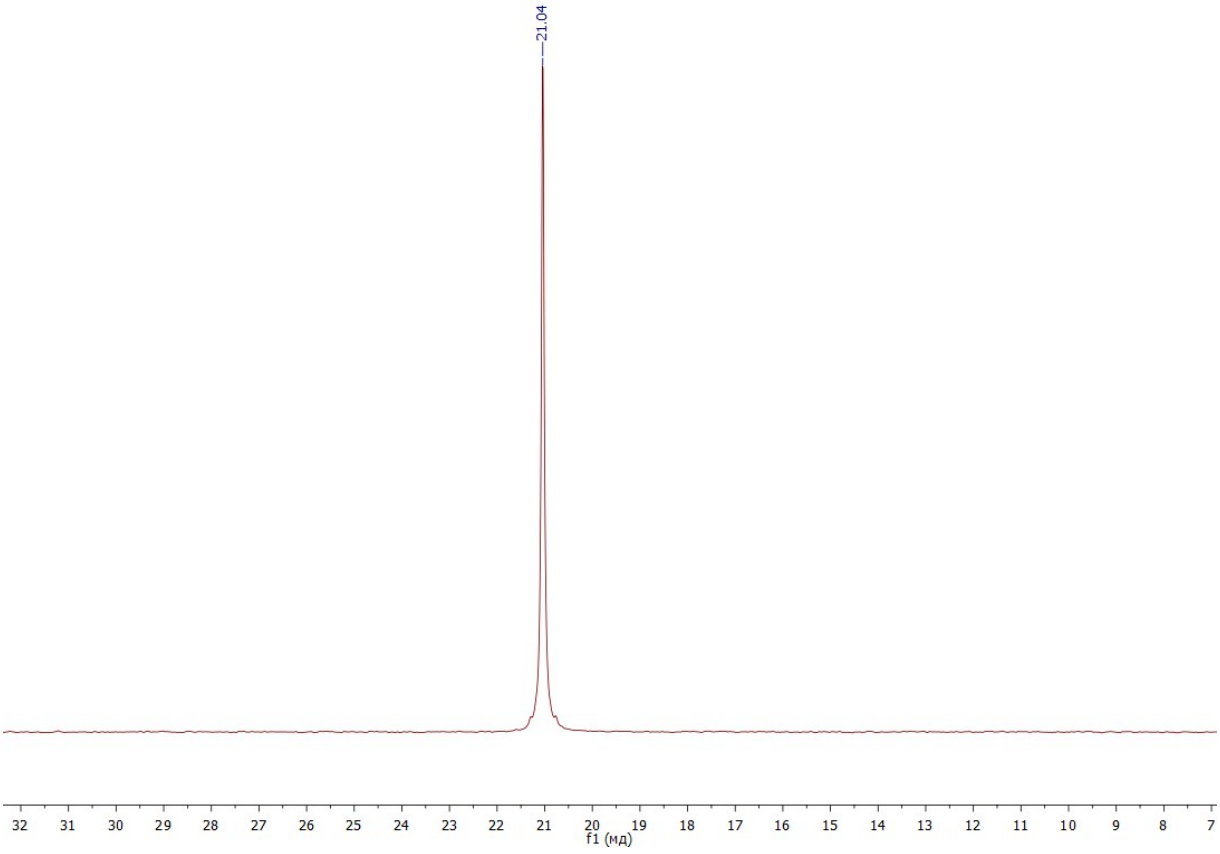

Figure S10. $^{31}P\{^{1}H\}$ NMR spectrum of 1,7-bis(diphenylphosphinyl)-*m*-carborane (L) ($CDCl_3$).

§4. FT-IR spectra

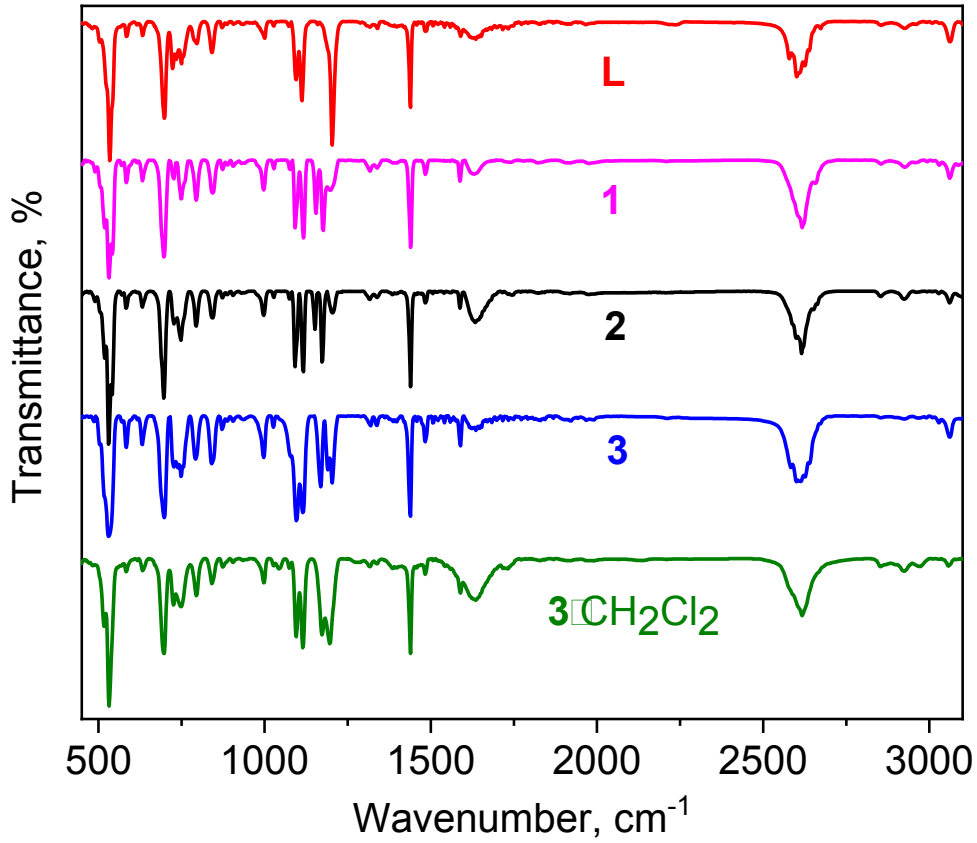

Figure S11. FT-IR spectra of **L**, CPs **1–3** and **3**·CH_2Cl_2 showed in the 500–3100 cm^{-1} region.

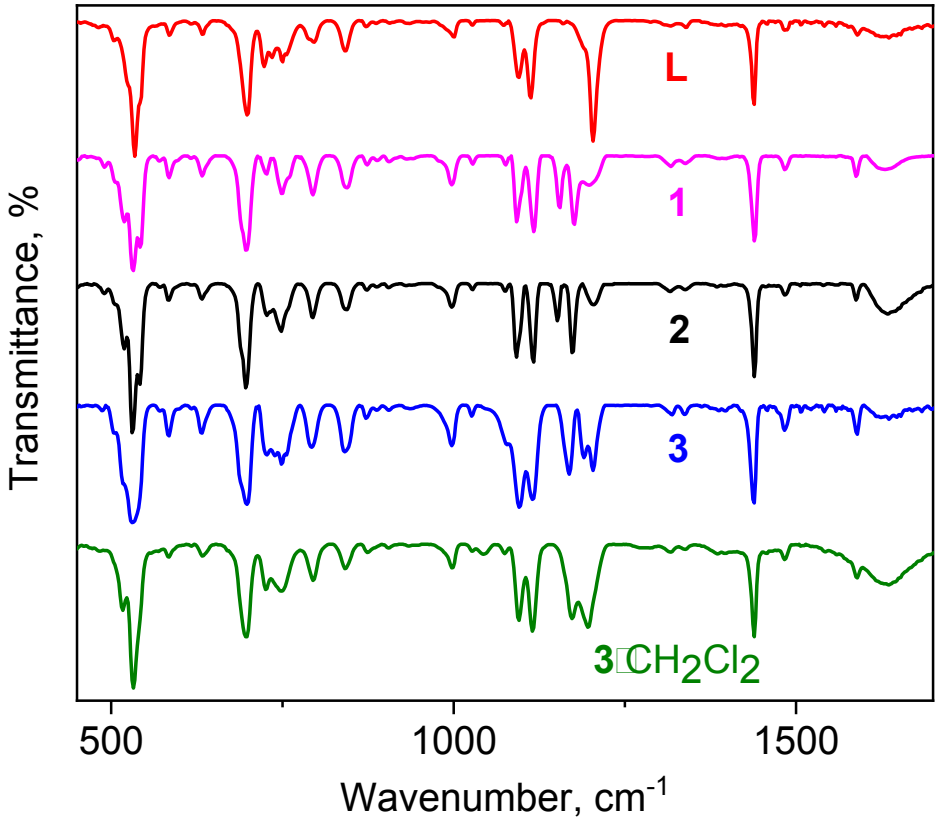

Figure S12. FT-IR spectra of **L**, CPs **1–3** and **3**·CH_2Cl_2 showed in the fingerprint region.

§5. Emission decay curves

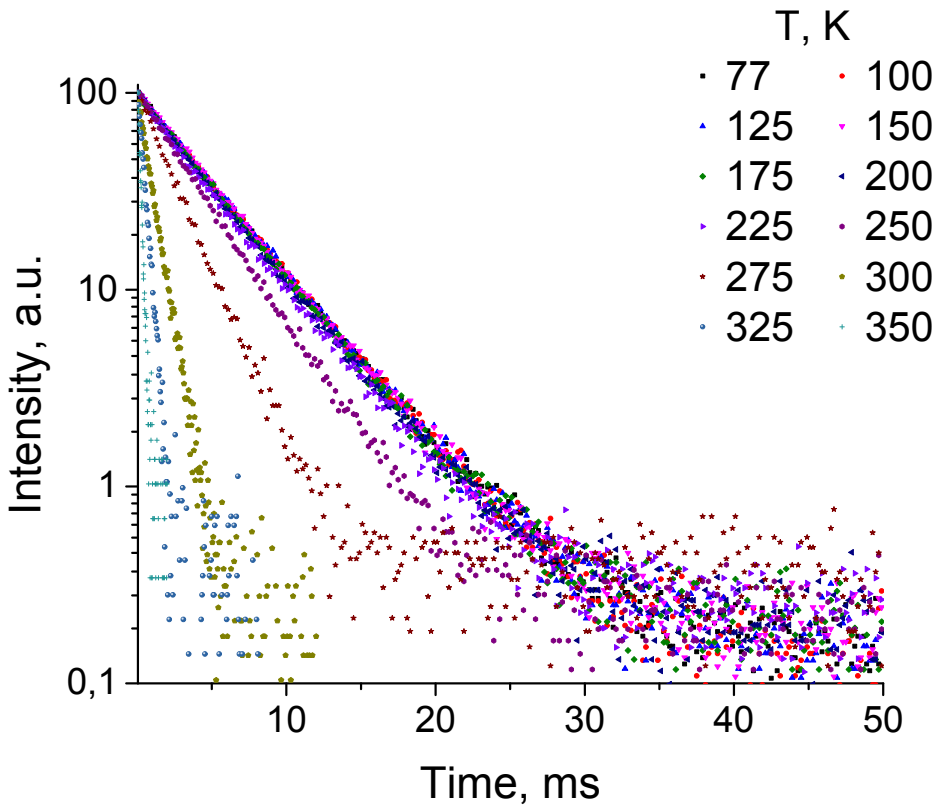

Figure S13. PL kinetic decays for CP **1** (λ_{Ex} = 438 nm, λ_{Em} = 515 nm).

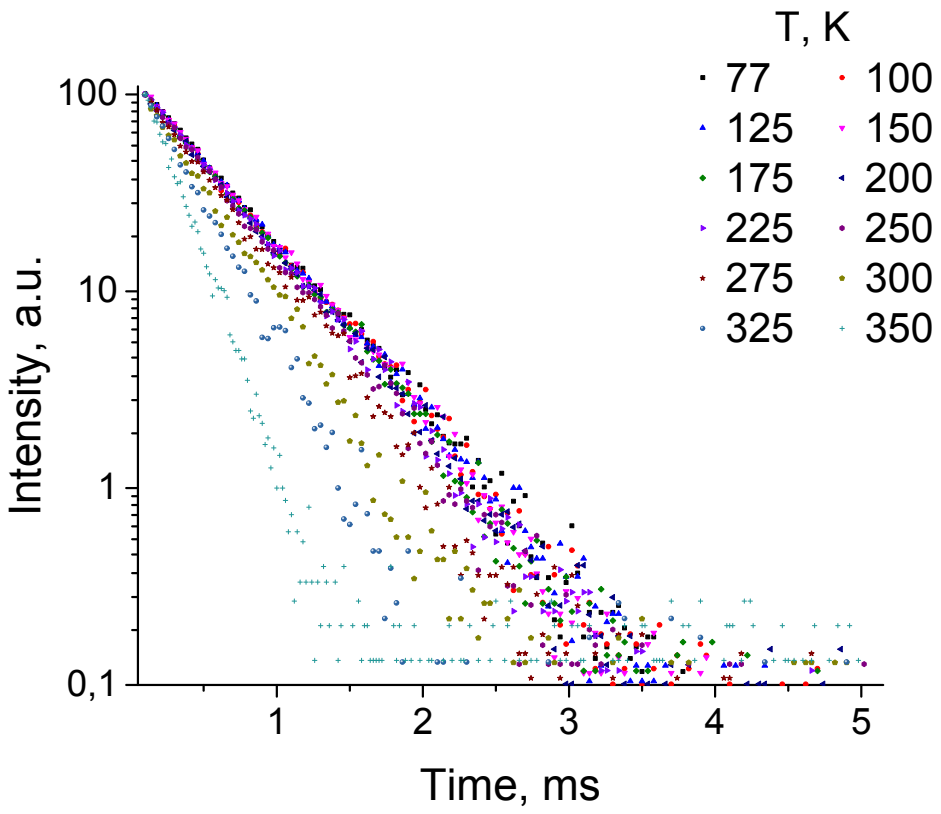

Figure S14. PL kinetic decays for CP **2** (λ_{Ex} = 422 nm, λ_{Em} = 520 nm).

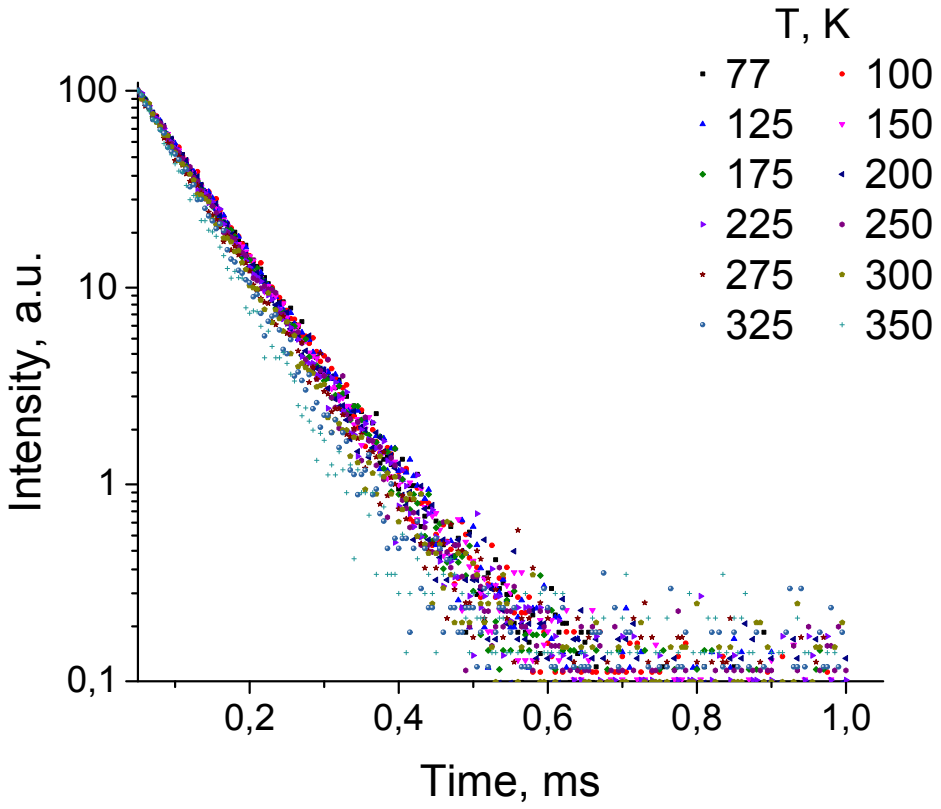

Figure S15. PL kinetic decays for CP **3** (λ_{Ex} = 460 nm, λ_{Em} = 560 nm).

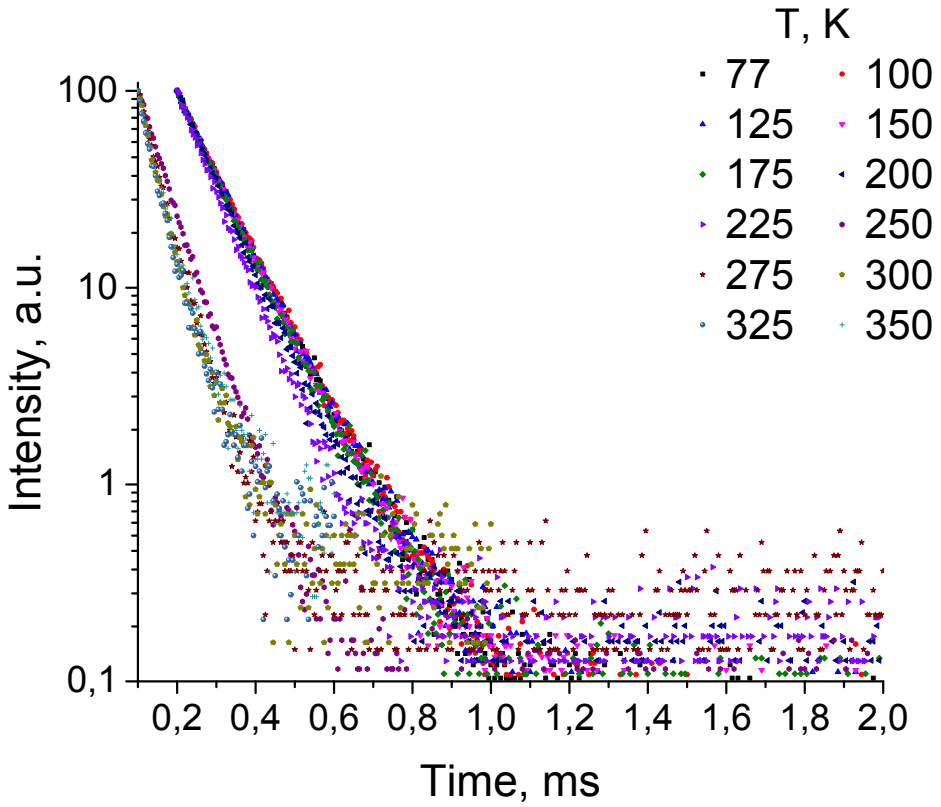

Figure S16. PL kinetic decays for CP **3**·CH_2Cl_2 (λ_{Ex} = 445 nm, λ_{Em} = 510 nm).

§6. Photostability data

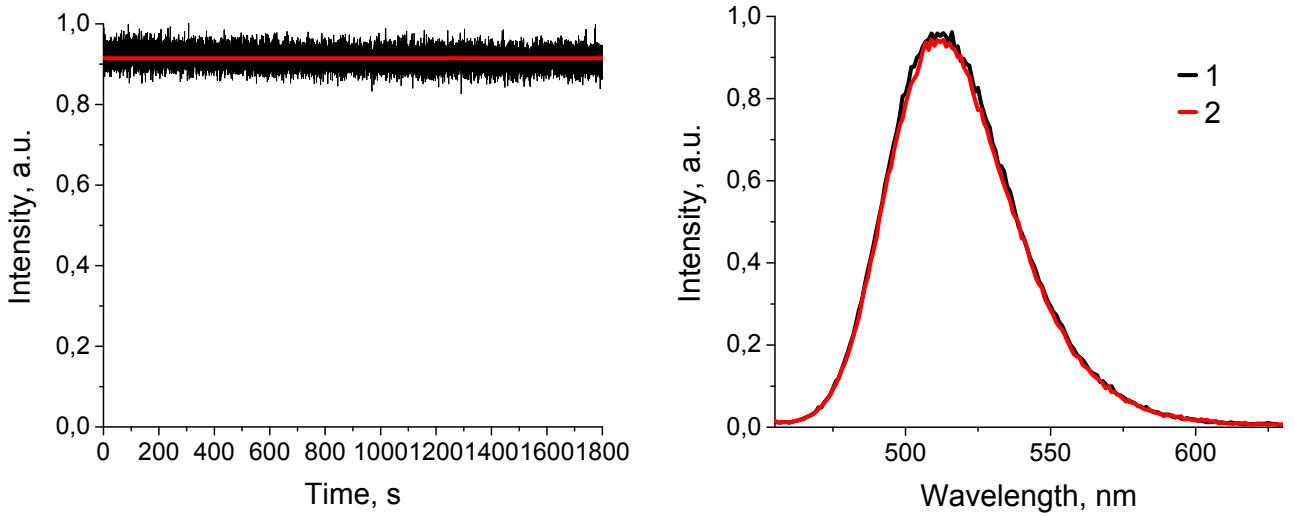

Figure S17. Photostability data for CP **1**. *Left*: Emission intensity against time (λ_{Ex} = 438 nm, λ_{Em} = 510 nm, r.t.). The red line is a fitting by the constant function. *Right*: Emission spectra before (1) and after (2) exposure on 438 nm light for 30 min.

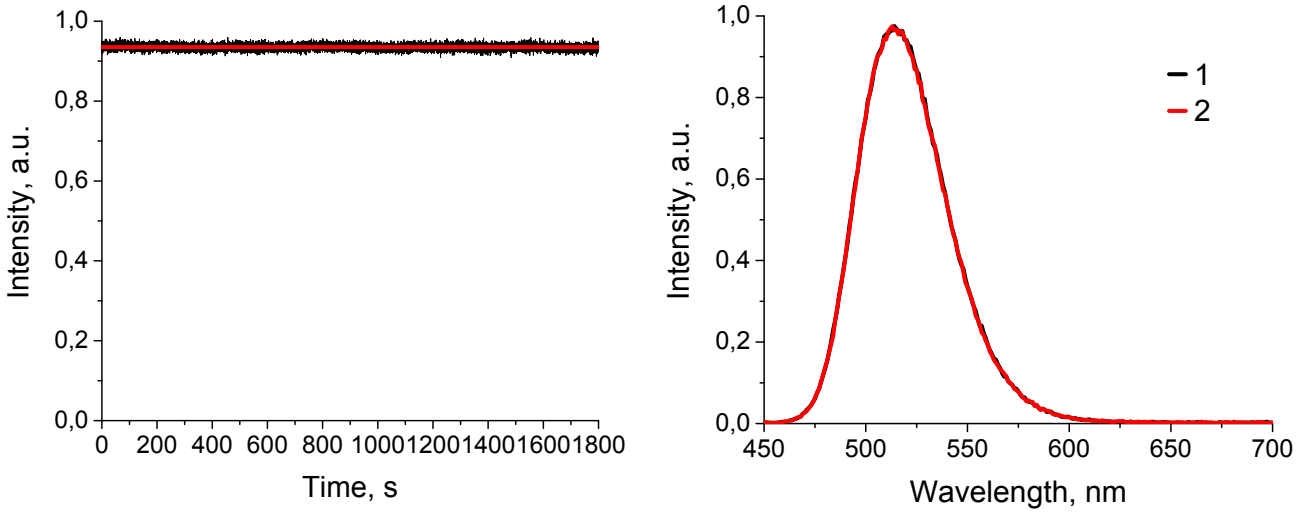

Figure S18. Photostability data for CP **2**. *Left*: Emission intensity against time (λ_{Ex} = 422 nm, λ_{Em} = 510 nm, r.t.). The red line is a fitting by the constant function. *Right*: Emission spectra before (1) and after (2) exposure on 422 nm light for 30 min.

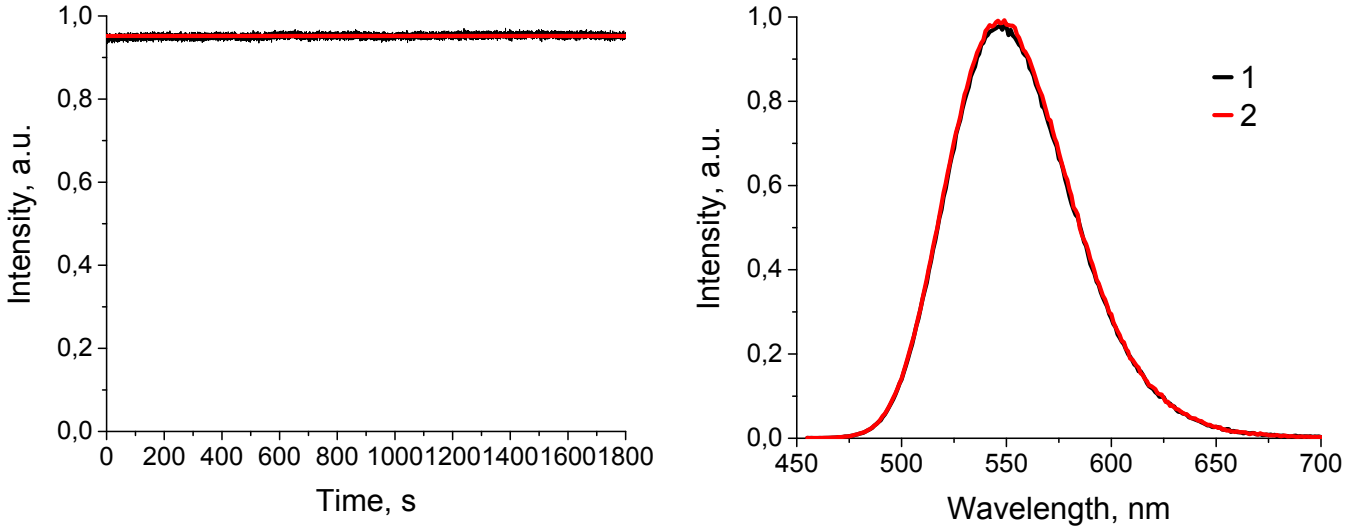

Figure S19. Photostability data for CP **3**. *Left*: Emission intensity against time (λ_{Ex} = 460 nm, λ_{Em} = 546 nm, r.t.). The red line is a fitting by the constant function. *Right*: Emission spectra before (1) and after (2) exposure on 460 nm light for 30 min.

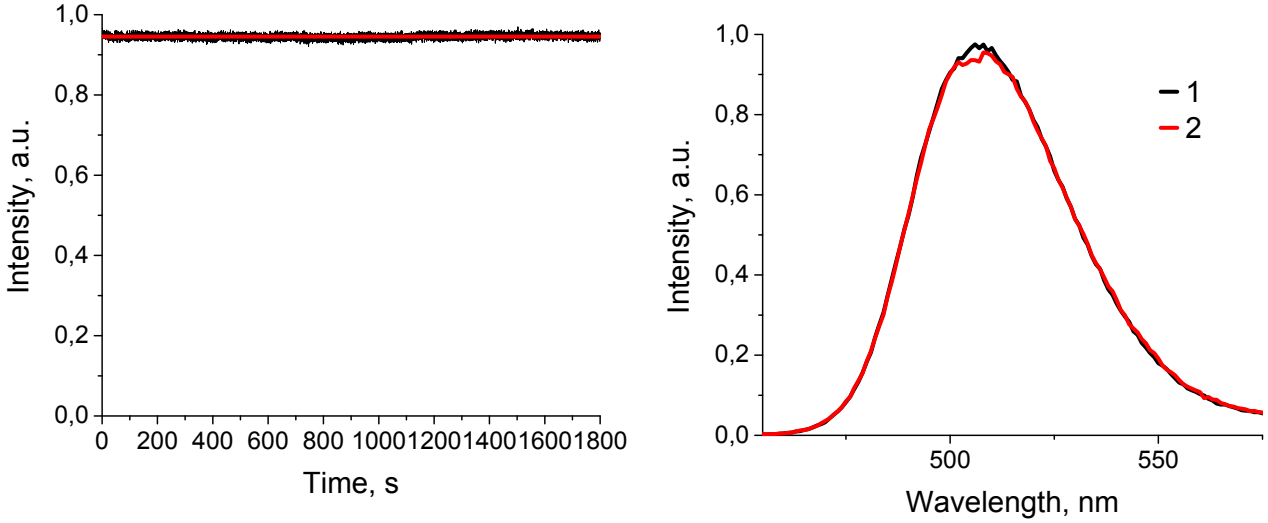

Figure S20. Photostability data for CP **3**·CH_2Cl_2. *Left*: Emission intensity against time (λ_{Ex} = 442 nm, λ_{Em} = 507 nm, r.t.). The red line is a fitting by the constant function. *Right*: Emission spectra before (1) and after (2) exposure on 442 nm light for 30 min.

§7. Photophysical data for ligand L

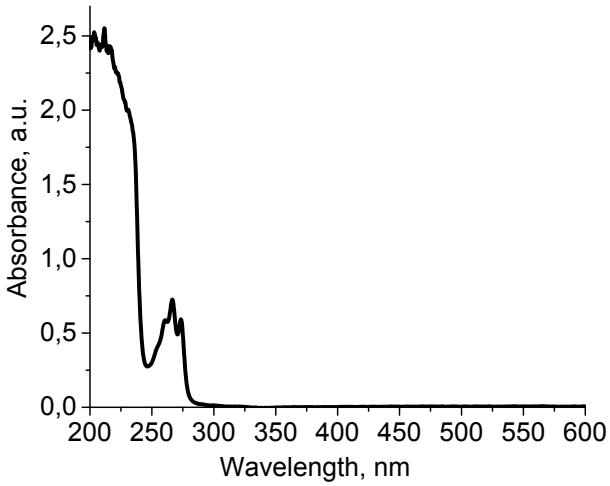

Figure S21. UV-Vis absorption spectrum of the ligand L recorded in MeCN solution at 25 °C.

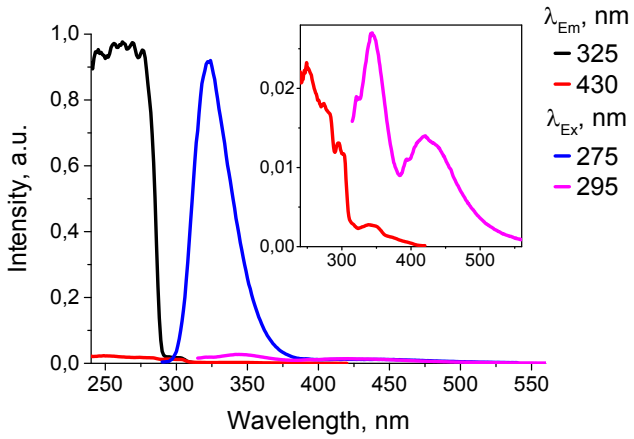

Figure S22. Steady-state excitation and emission spectra of the ligand L at 77 K.

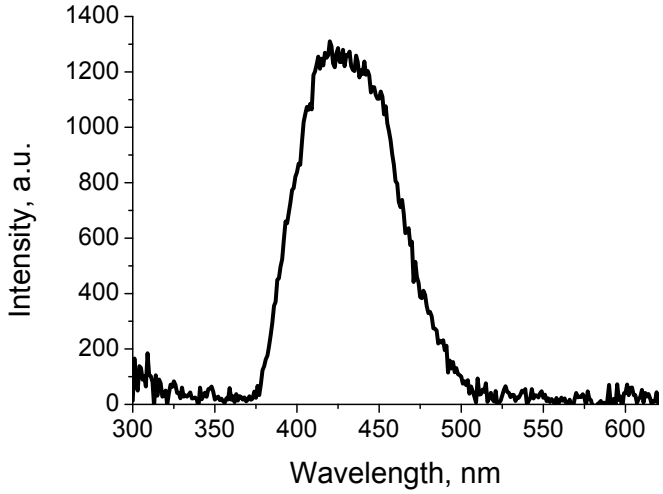

Figure S23. Time-resolved PL spectrum of the ligand recorded at 77 K with time delay of 100 ms (λ_{ex} = 300 nm).

The T_1 state energy of the ligand has been evaluated as follows. The excitation and emission maxima, corresponding to the S_1–S_0 transitions, are 36400 cm^{-1} and 30800 cm^{-1}, respectively. Thus, the Stokes shift is 5600 cm^{-1}, and the 0–0 transition energy can be estimated as 33600 cm^{-1}. Assuming a similar Stokes shift for the phosphorescence, the energy of 0–0 transition between T_1 and S_0 states can be estimated as 26600 cm^{-1}.

§8. DFT study of the ligand

DFT calculations of 1,7-bis(diphenylphosphinyl)-*m*-carborane (L) were carried out using Gaussian 09 suite.[6] The structures of the S_0 and T_1 states were fully optimized using PBE1PBE[7,8] and B3LYP[9] functionals coupled with the def2-TZVPPD basis set.[10] There are no imaginary frequencies in all optimized structures. The calculated IR spectrum, multiplied by a scaling factor of 0.98, well agrees with the experimental one in the fingerprint range (Fig. S24). The calculated $\nu_{B\text{-}H}$ stretching vibrations, however, are shifted in high frequency domain as competed to the experimental bands.

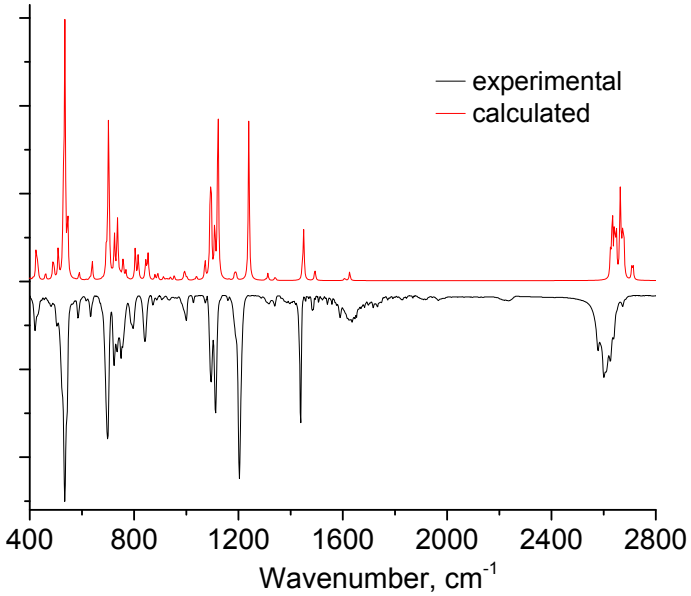

Figure S24. The calculated and experimental IR spectra of 1,7-bis(diphenylphosphinyl)-*m*-carborane (L).

The overlayed structures of the T_1 and S_0 states are plotted in Figure S25 illustrating geometric reorganization induced by the $S_0 \rightarrow T_1$ excitation. The most significant distortion concerns a phenyl ring that, upon excitation, becomes nonplanar and bent. At PBE1PBE/def2-TZVPPD theory level, the energy difference between the optimized T_1 and S_0 states is 28258 cm^{-1}. The close value of 28518 cm^{-1} has been obtained using B3LYP functional coupled with the same basis set.

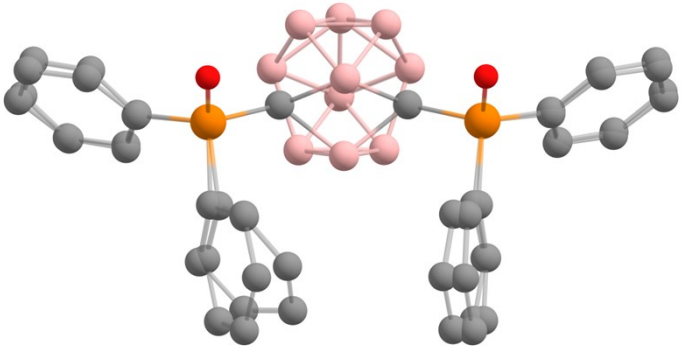

Figure S25. The overlayed structure of the ligand in its S_0 and T_1 states.

§9. Solvatochromic luminescence of 3·CH_2Cl_2

The desolvated CP **3A** has been obtained by heating of **3**·CH_2Cl_2 at 150 °C under vacuum for 10 min. Taking into account that **3A** and **3**·CH_2Cl_2 display nearly the same IR profiles, it can be concluded that their 1D chains are similar in terms of chemical bonding. Figure S26 display PXRD patterns for the parent CP **3**·CH_2Cl_2, desolvated CP 3A, and recovered solvate **3**·CH_2Cl_2. The following conclusions can be drawn from these data:

(*i*) although sample 3A is significantly amorphized, the presence of apparent XRD reflexes implies a partial retention of the structured integrity. Probably, removing of the solvate molecules from 3·CH_2Cl_2 leads to a partial disordering of 1D polymer $[Mn(L)I_2]_n$ chains.

(*ii*) The fuming of 3A with CH_2Cl_2 vapors leads to the recovery of 3·CH_2Cl_2, i.e. the polymer $[Mn(L)I_2]_n$ chains become again structured ones. The emission characteristics of the parent and recovered samples of **3**·CH_2Cl_2 are very similar.

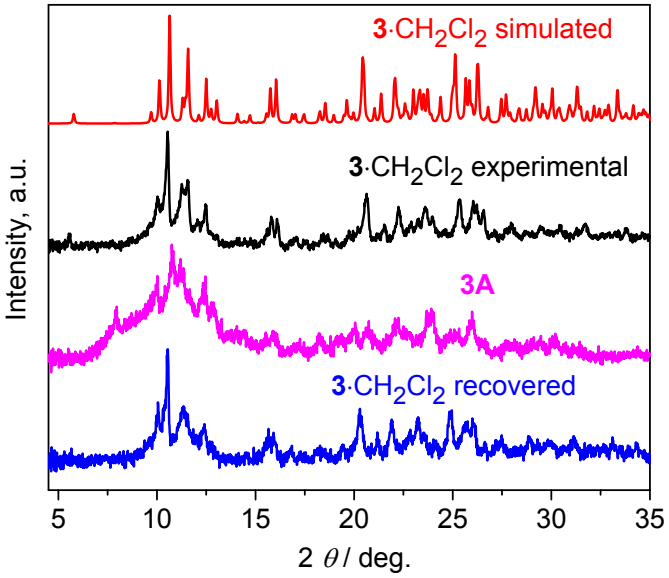

Figure S26. PXRD patterns for the parent solvate **3**·CH_2Cl_2, desolvated sample (**3A**), and recovered **3**·CH_2Cl_2.

Like to **3**·CH_2Cl_2, the emission of **3A** strongly enhances in its intensity upon cooling from 350 to 77 K (Fig. S27a). At that, the emission maximum of **3A** demonstrates bathochromic shift of about 10 nm, which is intermediate between that of parent **3**·CH_2Cl_2 ($\Delta\lambda_{max} \approx 3$ nm) and **3** ($\Delta\lambda_{max} \approx 17$ nm). The excitation pattern of **3A** resembles that of **3**·CH_2Cl_2 (Fig. S27b). The PL lifetime values of **3A** are very close to those of related CPs **3** and **3**·CH_2Cl_2 (Fig. S27c). Again, the PL thermal quenching energy (ΔE_{TQ}) of **3A** estimated from the τ(T) datasets (Fig. S27c) being 1500 K is consistent with such for **3** and **3**·CH_2Cl_2 (Table 1).

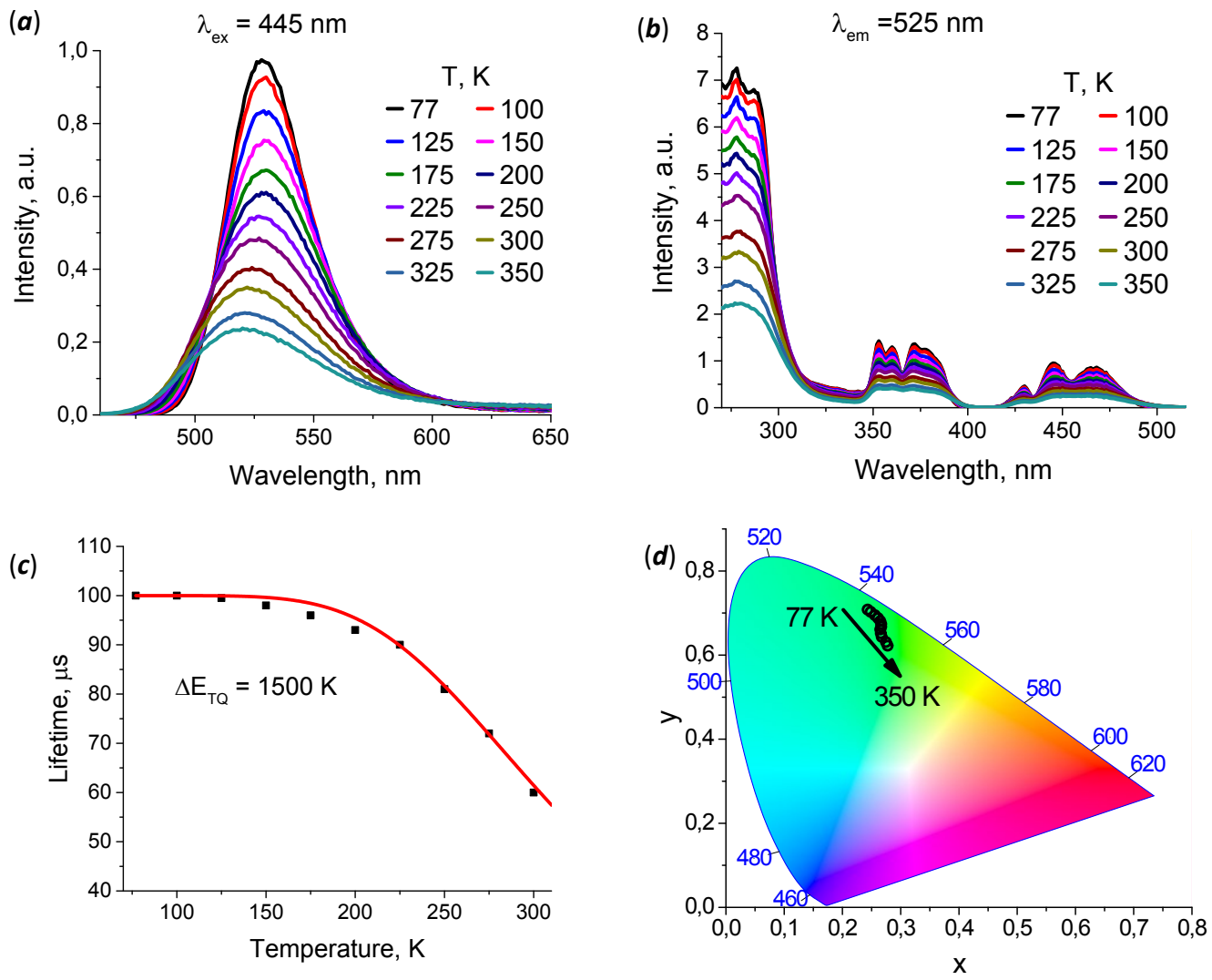

Figure S27. Photophysical data for **3A**: (***a***) emission spectra; (***b***) excitation spectra; (***c***) lifetime against temperature plot (λ_{ex} = 445 nm, λ_{em} = 525 nm); (***d***) CIE diagram showing temperature dependance of the emission chromaticity (λ_{ex} = 445 nm).

EPR spectrum of solid sample **3A** (Fig. S28) resembles that of parent solvate **3**·CH_2Cl_2 (Fig. 4 in the main document). The EPR parameters of **3A** are comparable with those of related MnI_2-based CPs **3** and **3**·CH_2Cl_2 (Table S2).

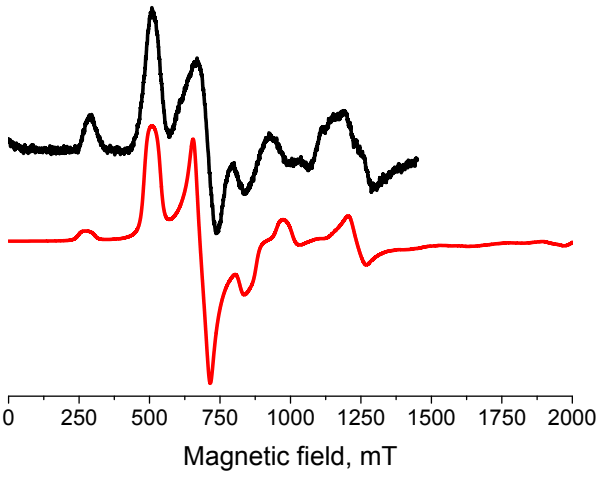

Figure S28. Q-band EPR spectrum of solid **3A** (black line – experimental, red line – the best fit of the experimental data).

Table S2. Experimental and calculated EPR parameters for solid MnI_2-based CPs **3**, **3**·CH_2Cl_2, and **3A**.

	3	**3**·CH_2Cl_2	**3A**
S	5/2	5/2	5/2
g	2.00	2.00	2.00
$\|D\|$ [MHz][a]	25760	39760	>45000
$\|E\|$ [MHz][a]	7000	8350	>9900
η[b]	0.26	0.21	0.22

[a] D and E – zero-field splitting (ZFS) parameters;
[b] $\eta = E/D$.

The DSC curves for CPs **3** and **3**·CH_2Cl_2 recorded in the 20−180 °C window are plotted in Figure S29. As seen from these data, no phase transformations take place for these compounds in the temperature range of 20−140 °C. The DSC curve of **3**·CH_2Cl_2 clearly presents an irreversible peak at ~ 160 °C assigned to the removal of the solvate molecules. In general, the DCS results well agree with the TGA/DTG data (Fig. 3).

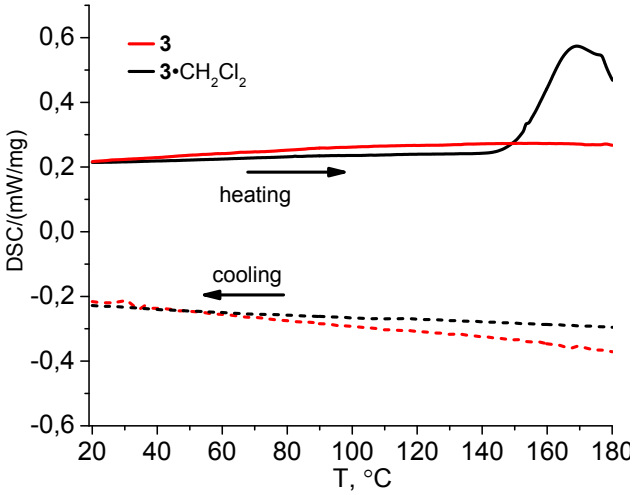

Figure S29. DSC curves for CPs **3** and **3**·CH_2Cl_2.

§10. References

[1] *CrysAlisPro 1.171.38.46*, Rigaku Oxford Diffraction: 2015.
[2] *Bruker Apex3 software suite: Apex3, SADABS-2016/2 and SAINT*, version 2018.7-2; Bruker AXS Inc.: Madison, WI, 2017.
[3] G.M. Sheldrick, *Acta Cryst. A*, 2015, **71**, 3–8.
[4] G.M. Sheldrick, *Acta Cryst. C*, 2015, **71**, 3–8.
[5] S. Parsons, H.D. Flack, T. Wagner, *Acta Cryst.* 2013, **B69**, 249–259.
[6] M. Frisch, G.W. Trucks, H.B. Schlegel, G.E. Scuseria, M.A. Robb, J.R. Cheeseman, G. Scalmani, V. Barone, B. Mennucci, Ga. Petersson, others, Gaussian 09, revision D. 01, (2009).
[7] C. Adamo, V. Barone, *J. Chem. Phys*., 1999, **110**, 6158–6170.
[8] J.P. Perdew, K. Burke, M. Ernzerhof, *Phys. Rev. Lett*., 1996, **77**, 3865–3868.
[9] P.J. Stephens, F.J. Devlin, C.F. Chabalowski, M.J. Frisch, *J. Chem. Phys*., 1994, **98**, 11623–11627.
[10] B.P. Pritchard, D. Altarawy, B. Didier, T.D. Gibson, T.L. Windus, *J. Chem. Inf. Model*., 2019, **59**, 4814–4820.